



MEC-Assisted Real-Time Data Acquisition and Processing for UAV With General Missions

Yao Zeng , *Student Member, IEEE*, and Jianhua Tang , *Member, IEEE*

Abstract—As a promising technology, unmanned aerial vehicles (UAVs)-enabled information gathering has received intensive interest in both academia and industry in recent years. However, the familiar paradigm, namely, data collection can hardly fulfill the active and real-time information gathering demands of many thriving smart applications, such as smart grid, where the UAV needs to serve as an intelligent aerial entity, gathering and analysing the information of surroundings actively and timely. To this aim, this article studies the paradigm *data acquisition*, where the UAV dynamically gathers information by on-board sensors. We consider a general mission scenario where a UAV acquires data in real time, which needs to be timely processed with the assistance of a mobile edge computing server. To address the real-time characteristics, we construct a novel theoretical *data acquisition rate* model, based on which the real-time processing quality of requirement (QoR) is defined. We respectively minimize the UAV energy consumption and mission completion time, under the constraints including real-time processing QoR and UAV mobility, by jointly optimizing the UAV trajectory, resources allocation, and time duration. To tackle these highly complex problems, we propose efficient algorithms by means of successive convex approximation and block coordinates descent techniques, where a closed-form solution for the UAV transmission and computation resources allocation is rigorously derived. Moreover, we consider a practical multi-location trajectory optimization where the UAV needs to traverse multiple target locations or areas in addition to the initial and final locations. The simulation results demonstrate the significant system performance gains brought by the proposed design and the effectiveness of the algorithms.

Index Terms—Data acquisition, data processing, mobile edge computing, trajectory optimization, unmanned aerial vehicles.

I. INTRODUCTION

DUE to a lot of merits, such as highly agile mobility, ease of deployment, and low cost of use, unmanned aerial

vehicles (UAVs) have received extensive appreciation from a wide spectrum of applications during the past few years [2], [3], [4], such as cargo delivery, aerial photography, communication cover, etc.

Among the various applications, UAV-aided information gathering has been considered as a promising one recently, where UAV is dispatched to gather data through numerous kinds of sensors for further processing. Preliminary field trials have extensively studied the paradigm *data collection* (DC), where UAV acts as a data mule, travelling or hovering above a sensor network composed of many Internet of Things (IoT) devices, which sense their surroundings and store data waiting to be collected by UAV [5]. In addition, there is another paradigm *data acquisition* (DA), where the UAV, as a sensor itself, gathers both its internal and external information timely, such as motion status, localizations, thermal images, videos, point clouds, etc. UAV DA can be classified into non-contacting UAV DA and contacting UAV DA. Except for some cases that only require simple sensors and interactions, such as air quality DA, the contacting UAV DA usually requires specialized mechanisms and sensor designs, e.g., aerial manipulator system, according to the specific physical interaction situations [6], [7], [8]. In this article, we mainly focus on non-contacting UAV DA, since the contacting UAV DA normally results in use-case-based models (depending on the contacting mechanisms and tasks), and cannot achieve a general model.

From the perspective of UAV, the difference between DC and DA generally lies in: 1) DC is passive while DA is active. This is because the data to be gathered in DA is directly sensed by UAV itself, whereas in DC, one is sensed by off-board sensors; 2) DC is static while DA is dynamic in both time and space. In DC, the data could be stored in sensors temporarily within a tolerance time before being gathered, whereas the data gathering in DA is real-time. Besides, the sensors in DC are generally fixed at some given locations with low mobility. However, in DA, the UAV can move freely to gather data flexibly.

Thanks to recent technical advancements, UAV is becoming increasingly autonomous and intelligent to assist in many thriving smart applications, such as smart agriculture [9], intelligent transportation systems (ITS) [10], smart grid [11], etc. In these applications, UAV can serve as an intelligent aerial entity, which actively acquires surroundings information and then makes real-time analyses and decisions. For instance, in ITS, UAV can be dispatched to provide real-time traffic parameters estimation from a top-view perspective [10] by shooting and analysing videos, where the abnormal information such as violations or

Manuscript received 8 March 2022; revised 8 June 2022; accepted 23 August 2022. Date of publication 2 September 2022; date of current version 16 January 2023. This work was supported in part by the National Nature Science Foundation of China under Grant 62001168 and in part by the Foundation and Application Research Grant of Guangzhou under Grant 202102020515. Part of this paper [1] will be presented at the 2022 IEEE Global Communications Conference (GLOBECOM), Rio de Janeiro, Brazil, December 2022. The review of this article was coordinated by Prof. Jalel Ben-Othman. (*Corresponding author: Jianhua Tang.*)

Yao Zeng is with the Shien-Ming Wu School of Intelligent Engineering, South China University of Technology, Guangzhou, Guangdong 510641, China (e-mail: yao_zeng_scut@outlook.com).

Jianhua Tang is with the Shien-Ming Wu School of Intelligent Engineering, South China University of Technology, Guangzhou, Guangdong 510641, China, and also with the Pazhou Lab, Guangzhou 510335, China (e-mail: jtang4@e.ntu.edu.sg).

Digital Object Identifier 10.1109/TVT.2022.3203704

incidents should be timely sent to corresponding road units to avoid accidents.

As one can see, data acquisition and processing are two of the crucial pillars for enabling these cases. However, the traditional methods in UAV DC cannot be directly utilized here due to the active and real-time information acquisition requirements. Therefore, new approaches are needed for such demands. Motivated by this, this work considers a real-time UAV data acquisition and processing scenario that can be applied in *general missions*. Specifically, we dispatch a UAV to fly through some given target locations, where it needs to timely acquire and process the information of surroundings during the entire flying. The meanings of *general missions* are threefold: 1) The amount of data to be acquired and processed is not predefined. Besides, the type of acquired data is not specified either, which can be video, point cloud, thermal image, etc, based on the practical demands; 2) The mission completion time (MCT) is not predefined; 3) The UAV needs to fly along a general trajectory that contains many extra target locations in addition to the initial and final locations. Considering the potential conflicts between the intensive computation requirements and limited on-board resources, we adopt the mobile edge computing (MEC) technology to boost the UAV performance.

Such a system design possesses high complexity. Firstly, in order to characterize the real-time demands, a challenge thus comes in modeling the real-time data acquisition and processing procedures, which are related to the time-varying variables such as the UAV motion and location status, system resources, etc. Another challenge is how to dispatch UAV to fully harness the advantages offered by the MEC server. A well-designed UAV trajectory is needed to improve the UAV performance by sufficiently exploiting the UAV mobility. Besides, UAV needs to strike an optimal balance between offloading or locally processing the tasks, since a poor tasks allocation can result in a considerable system performance degradation.

A. Related Works

There has been a great number of works about the UAV DC in the communication area with different optimization objectives. 1) For the MCT issues, [12] studies a scenario where a UAV collects data from a set of sensor nodes (SNs) on a straight line, where the MCT is minimized. In [13], the UAV altitude is considered to enlarge the transmission radius, which can further decrease trajectory length and MCT. [14] minimized the maximum MCT among a UAV swarm, where the SNs energy budget is considered; 2) For the energy issues, [15] investigates the energy tradeoff between the UAV swarm and SNs. [16] studies an energy-efficient route planning problem for both a UAV collecting data and a mobile charging station by means of deep reinforcement learning (DRL). [17] minimizes the maximum energy consumption of all SNs by optimizing the SNs wake-up scheduling and UAV trajectory. [18] considers a dynamic and heterogeneous SNs scenario; 3) For the quality of service (QoS) issues, [19] maximizes the minimum average data collection rate from all SNs, where a three-dimensional (3D) UAV trajectory optimization and angle-dependent Rician fading channel are

considered. [20] maximizes the number of served SNs, which have different target data upload deadlines. In [21], the average age of information (AoI) of collected data is minimized, where the wireless energy transfer is also considered.

UAV DA has attracted a great deal of attention in a wide range of areas, such as agriculture, smart grid, ITS, communication, etc. For example, in the field of agriculture, UAV DA can be used in crop monitoring [9], [22], [23], plant detecting [24], crop protection [25], etc. In the field of smart grid, UAV DA can assist power line inspection [11], power network damage assessment [26], etc. In the field of ITS, UAV DA can be applied in traffic parameter detection and estimation [10], [27], [28], [29]. [30] considers a UAV-aided mobile crowd sensing system, where the authors maximize a profit which is related to UAV data acquisition latency, quality, and quantity. In [31], a UAV needs to acquire information at several locations, where the authors formulate a UAV routing problem to minimize the MCT. [32] considers a similar scenario with [31], where a tradeoff between the UAV sensing and communication is studied to minimize the AoI. In the more relevant area, recently, [1] considers a dynamic UAV DA scenario and minimizes the UAV energy consumption, where the UAV only traverses two target locations.

Nevertheless, the dynamic characteristics of DA in works [30], [31], [32] are not well addressed in these works for two reasons: 1) In the previous works, the amount of data to be acquired is pre-determined. In fact, we can hardly determine it in advance due to the dynamic acquisition procedure; 2) In the previous works, data is only acquired at some specific locations. However, in many practical missions, the UAV needs to acquire the information during the entire flight to meet the real-time demands, such as autonomous flying, target tracking, search-and-rescue [33], etc.

MEC-assisted UAVs (referred to as UAV-MEC below) system is receiving intensive attention, due to the ability to alleviate the conflicts between the demanding computing requirements and insufficient on-board resources. [34] studies a UAV-MEC system containing multiple UAVs and one base station (BS) equipped with a MEC server. By jointly optimizing the task and resources allocation and the UAVs trajectories, this work minimizes the total UAVs energy consumption. Instead of directly optimizing the UAV trajectory, [35] optimizes it based on the perspective of optimal control theory. Nonetheless, only the longitudinal mobility of UAV is considered. [34] and [35] assume that the MCT is pre-determined. In [36], by optimizing the UAV trajectory and offloading scheduling, the authors minimize the MCT, where the UAV needs to offload a given amount of tasks to multiple MEC servers. Likewise, [37] also minimizes the MCT, where the authors consider a 3D trajectory optimization and propose an effective offloading area design in addition. However, the UAV energy consumption and local computing are not considered in [36] and [37]. Some works do not consider trajectory optimization. [38] addresses the system dynamics, where the offloading decisions depend on the current network system realization. [39] and [40] consider the energy-efficient offloading problems, emphasizing on the system secrecy, where an access point (AP) imposes artificial noise on an Eve during the UAV offloading. In addition, [41] considers a cloud-based

UAV system, where the system stability for data acquisition and processing is addressed by queuing theory.

Moreover, in the works mentioned above, the trajectory optimizations mainly focus on the two-location scenario, where the UAVs merely need to traverse a pair of target locations. In fact, UAV is often required to pass through many additional target locations or areas in practical missions, except for the initial and final locations, such as surveillance and monitoring [42]. There are only a few related works considering the multi-location scenario. [43] and [44] discuss the multi-location trajectory initialization methods. Nonetheless, the considered trajectories constitute only connected line segments, which are not flyable due to UAV kinetics constraints such as the minimum turn radius and maximum acceleration magnitude.

B. Contributions

In this article, we seek insights on the real-time UAV data acquisition and processing with the assistance of MEC in general missions. Specifically, our contributions are listed as follows:

- To address the real-time system characteristics, we construct a theoretical model of UAV *data acquisition rate* as a function of UAV speed, based on which a real-time data processing quality of requirement (QoR) is defined.
- For different mission demands, we respectively minimize the UAV energy consumption and MCT by taking full advantage of the MEC server resources, under the constraints including the real-time processing QoR, where the UAV transmission power, computation frequency, time duration, and trajectory are jointly optimized.
- Different from most works on trajectory optimization, we consider a more practical scenario, where the UAV needs to traverse multiple target locations. For this design, we put forward a systematic and generic method to obtain a smooth trajectory initialization by means of Dubins curves.
- We rigorously derive a closed-form optimal allocation for the UAV transmission and computation resources.
- Sufficient simulations have been conducted to verify the significant performance gain brought by our MEC-assisted UAV system design and the effectiveness of the proposed algorithms.

C. Organization

The rest of this article is organized as follows. In section II, we introduce our system model, and the energy minimization problem is formulated. In section III, we propose our algorithm for the energy minimization problem, where the multi-location trajectory initialization method is presented. The MCT minimization problem is formulated and solved in section IV. In section IV-A, we discuss the implementation of the proposed system briefly. In section V, the system performance gain and the effectiveness of the proposed algorithms are illustrated. Finally, we draw the conclusions in section VI.

Notations: We use $\dot{\mathbf{q}}(t)$ and $\ddot{\mathbf{q}}(t)$ to denote the first and second derivative of $\mathbf{q}(t)$ with respect to (w.r.t.) t . We employ \succeq and \succ to respectively denote the entrywise inequality and entrywise strict inequality between vectors.

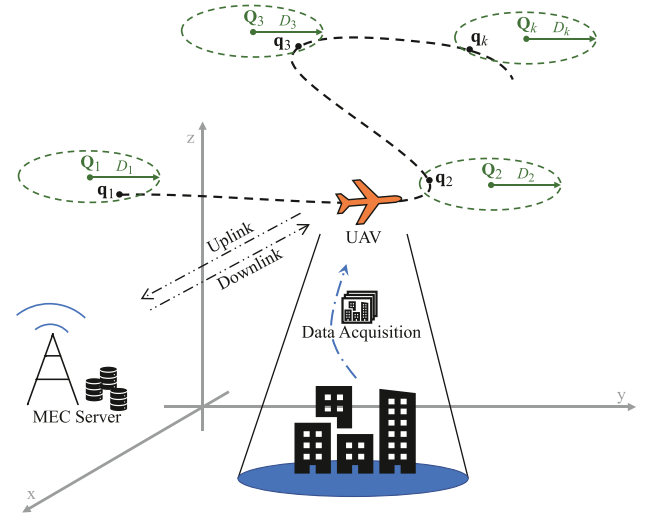


Fig. 1. UAV-BS system.

II. SYSTEM MODEL AND PROBLEM FORMULATION

A. System Model

As shown in Fig. 1, we consider a system that contains one fixed-wing UAV¹ and one BS equipped with an MEC server. The UAV is employed to visit K target locations in a pre-defined order. The horizontal coordinates of these target locations are denoted by $\mathbf{Q}_k \in \mathbb{R}^{2 \times 1}$, for $k = 1, \dots, K$. For each location k , we consider a corresponding disk area, centered at \mathbf{Q}_k , with pre-defined radius D_k . If the UAV flies into the disk area of location k , we regard a successful visitation for target location \mathbf{Q}_k . Hence, there should be at least K locations $\{\mathbf{q}_k\}$ on the UAV trajectory to ensure the visitation, which satisfy $\|\mathbf{q}_k - \mathbf{Q}_k\|_2 \leq D_k$, $\forall k = 1, 2, \dots, K$. We refer to \mathbf{q}_k as *visitation location*, where \mathbf{q}_1 denotes the starting visitation location, which is pre-defined. During the flying, UAV acquires data and generates delay-sensitive tasks dynamically. However, due to the limited on-board energy and computation resources, UAV has to resort to the MEC server to fulfill the intensive computation requirements. It is worth mentioning that our setup is quite general, where each target location can correspond to the ground terminal, the target of interest, etc., and disk radius can thus correspond to the communication radius, camera coverage, error tolerance, etc.

We assume that the UAV flies at a constant altitude H above the BS, with the speed constraint from V_{min} to V_{max} and the maximum acceleration magnitude a_{max} constraint.

It is worth noting that the fixed-wing UAVs have different kinematic constraints with the rotary-wing UAVs, practically. In contrast to rotary-wing UAVs that are able to hover, fixed-wing UAVs must maintain a forward motion to keep aloft. Herein, the minimum speed V_{min} is for the fixed-wing UAV to remain aloft, which is also known as the stall speed [45]. The time it takes to fly from the starting visitation location \mathbf{q}_1 to the k -th visitation

¹A fixed-wing UAV is utilized here since its larger payload and endurance than those of a rotary-wing UAV in general. Furthermore, similar to [45], this work can be easily extended to the rotary-wing UAVs by accordingly modifying the energy consumption model and omitting the minimum speed constraint.

location \mathbf{q}_k is denoted by T_k . Hence, the MCT can be expressed as T_K . Denote the UAV trajectory projected onto the horizontal plane as $\mathbf{q}(t) = [x(t), y(t)]^T \in \mathbb{R}^{2 \times 1}$ with $0 \leq t \leq T_K$, and let $\mathbf{v}(t) \triangleq \dot{\mathbf{q}}(t)$ and $\mathbf{a}(t) \triangleq \dot{\mathbf{v}}(t)$ denote the instantaneous velocity and instantaneous acceleration of UAV, respectively. We then have $V_{min} \leq \|\mathbf{v}(t)\|_2 \leq V_{max}$ and $\|\mathbf{a}(t)\|_2 \leq a_{max}$. The time-varying distance from the UAV to the BS at any time instant $t \in [0, T_K]$ is given by $d(t) = \sqrt{H^2 + \|\mathbf{q}(t) - \mathbf{Q}_{BS}\|_2^2}$, where \mathbf{Q}_{BS} denotes the horizontal coordinate of the BS. We consider the case that the channel between the UAV and BS is dominated by line-of-sight (LoS) link as in [36], [45]. Moreover, we assume that the Doppler effect caused by the UAV mobility is perfectly compensated at the receiver as in [45]. Thus, at any time instant t , the channel follows the free-space path loss model, which can be described as

$$h(t) = \frac{\beta_0}{d(t)^2} = \frac{\beta_0}{H^2 + \|\mathbf{q}(t) - \mathbf{Q}_{BS}\|_2^2}, \quad (1)$$

where β_0 denotes the reference channel power gain at the distance of 1 m. Denote the UAV transmission power at time instant t as $p(t)$, for $0 \leq p(t) \leq P$, where P represents the maximum transmission power. Therefore, the channel capacity between BS and UAV at time instant t measured in bit/s is expressed as

$$\begin{aligned} R(t) &= B \log_2 \left(1 + \frac{p(t)h(t)}{\sigma^2} \right) \\ &= B \log_2 \left(1 + \frac{\gamma_0(t)}{H^2 + \|\mathbf{q}(t) - \mathbf{Q}_{BS}\|_2^2} \right), \end{aligned} \quad (2)$$

where B is the channel bandwidth, σ^2 is the white Gaussian noise power at the BS. At time instant t , the reference received signal-to-noise ratio (SNR) at the distance of 1 m is denoted by $\gamma_0(t) = \frac{p(t)\beta_0}{\sigma^2}$.

B. Data Acquisition and Processing Model

Naturally, for a sensor, the data acquisition procedures are normally dynamic, which are related to the surrounding environment and acquisition time horizon. The changing rate of the surrounding environment directly affects data acquisition in general. For instance, when surroundings change rapidly, the sensor should increase the sampling rate to guarantee the accurate perception of the external states. On this basis, we claim that the data acquisition rate should be positively associated with the UAV speed. For example, when a UAV is shooting a video, the frame rate of the video should be increased when the UAV is speeding up, so as to ensure the video definition and details. Hence, denoted by $\dot{\zeta}(t)$, the data acquisition rate (in bit/s) at time instant t is modeled as

$$\dot{\zeta}(t) = \Theta(\|\mathbf{v}(t)\|_2) > 0, \quad (3)$$

where $\Theta(\cdot) : \mathbb{R} \rightarrow \mathbb{R}$ is a monotonically non-decreasing convex and integrable function. To leave more space for applications and practice, here we do not restrict the specific expression of the function, which can be determined by an end user based on the practical mission demands.

For the acquired data, we aim to design a corresponding real-time processing mechanism. It means that at any time instant

t , the ability to process data should be no less than the data acquisition rate. The ability contains two parts:

- The ability to process data at the UAV. For the sake of energy-efficient computing, we adopt the dynamic voltage and frequency scaling (DVFS) technique for UAV. We denote the CPU frequency of UAV at time instant t as $f(t)$, for $0 \leq f(t) \leq F$, where F is the maximum allowable CPU frequency. Then the ability to process data at UAV is $f(t)/\eta$ (bit/s), where η denotes the number of required CPU cycles to process 1-bit data. We refer to the procedure of data processing at the UAV as *local computing*.
- The ability to process data at the MEC server. We assume that the MEC server always has enough computation capacity as long as it receives the data, and the time to send the result back to the UAV is negligible. Then the only bottleneck is the data uploading rate $R(t)$. Hence, we consider the ability to process data at the MEC server as $R(t)$.

In order to simplify the analysis, we assume that the acquired data is bitwise independent, which can be arbitrarily partitioned into subtasks. Assuming that all the acquired data should be processed instantly, we thus have the real-time processing QoR,

$$f(t)/\eta + R(t) \geq \dot{\zeta}(t), \quad \forall t \in [0, T_K].$$

C. Energy Consumption Model

The energy consumption of local computing E^c during time horizon T_K is given by [46]

$$E^c = \int_0^{T_K} L f(t)^3 dt, \quad (4)$$

where L is a constant depends on the practical chip architecture.

According to [47], the energy consumption for offloading during time horizon T_K is expressed as

$$E^o = \int_0^{T_K} (P_0 + c_p p(t)) dt, \quad (5)$$

where P_0 refers to the baseline power that has the transmission circuitry switched on, and c_p is a scale parameter measuring the communication energy consumption with the transmission power.

For fixed-wing UAV, the propulsion energy consumption E^p during time horizon T_K can be calculated as [45]

$$E^p = \int_0^{T_K} \left[c_1 \|\mathbf{v}(t)\|_2^3 + \frac{c_2}{\|\mathbf{v}(t)\|_2} \left(1 + \frac{\|\mathbf{a}(t)\|_2^2}{g^2} \right) \right] dt, \quad (6)$$

where c_1 and c_2 are the physical properties of the UAV, and g denotes the magnitude of gravity vector.

In general, the energy for data processing is much larger than the one for data acquisition, which is thus not considered for simplicity. Therefore, the total energy consumption of UAV is $E^c + E^p + E^o$.

D. Energy Minimization Problem Formulation

We aim to minimize the total energy consumption of UAV by jointly optimizing the UAV transmission power, CPU frequency,

trajectory and time duration. The energy minimization problem is formulated as

$$\begin{aligned}
 & \text{(P-1)} \quad \min_{p(t), f(t), \mathbf{q}(t), T_K} E^c + E^p + E^o \\
 & \text{s.t.} \quad f(t)/\eta + R(t) \geq \dot{\zeta}(t), \quad \forall t \in [0, T_K], \quad (7) \\
 & \quad 0 \leq p(t) \leq P, \quad \forall t \in [0, T_K], \quad (8) \\
 & \quad 0 \leq f(t) \leq F, \quad \forall t \in [0, T_K], \quad (9) \\
 & \quad \mathbf{v}(t) = \dot{\mathbf{q}}(t), \quad \forall t \in [0, T_K], \quad (10) \\
 & \quad V_{\min} \leq \|\mathbf{v}(t)\|_2 \leq V_{\max}, \quad \forall t \in [0, T_K], \quad (11) \\
 & \quad \mathbf{a}(t) = \ddot{\mathbf{q}}(t), \quad \forall t \in [0, T_K], \quad (12) \\
 & \quad \|\mathbf{a}(t)\|_2 \leq a_{\max}, \quad \forall t \in [0, T_K], \quad (13) \\
 & \quad \|\mathbf{q}_k - \mathbf{Q}_k\|_2 \leq D_k, \quad \forall k = 1, 2, \dots, K. \quad (14)
 \end{aligned}$$

Problem (P-1) is hard to tackle, because of the coupled continuous-time variables in the integral terms and the unknown MCT T_K . In the following section, we propose a tractable way to solve this problem.

III. PROPOSED SOLUTION

First of all, to handle the difficulties brought by the continuous-time variables, we employ the *path discretization* technique [48]. Herein, it is necessary to clarify the terminologies of *trajectory* and *path*. In general, a *trajectory* is a vector function, whose domain is time and the range is the coordinate vectors. However, a *path* only specifies the coordinate vectors and does not involve the time dimension. In particular, the discretization procedures are as follows:

- Firstly, we discretize the path of UAV into many line segments, which are characterized by many discrete waypoints $\mathbf{q}[n]$. For each sub-path between two adjacent visitation locations, the number of line segments are predefined and fixed. That is, we introduce a series of predefined constants N_k to indicate that the UAV visits target location \mathbf{Q}_k at the N_k -th waypoint $\mathbf{q}[N_k]$, for $k = 1, 2, \dots, K$. We thus have $\hat{N} \triangleq N_K - 1$ line segments in total, and the visitation location \mathbf{q}_k is rewritten as $\mathbf{q}[N_k]$. Therefore, trajectory $\mathbf{q}(t)$, for $0 \leq t \leq T_K$, is approximated as $\mathbf{q}[n]$, for $n = 1, 2, \dots, N_K$, where $\mathbf{q}[1] \triangleq \mathbf{q}_1$ is a pre-determined UAV initial location.
- In addition, we introduce a parameter Δ . When $\|\mathbf{q}[n+1] - \mathbf{q}[n]\|_2 \leq \Delta$, $\forall n = 1, 2, \dots, \hat{N}$, and Δ is small enough, the time-varying variables, such as UAV speed and channel condition, are regarded as unchanged in $t[n]^2$.

²This work mainly focuses on the environments where two adjacent target locations are far enough from each other, i.e., $\|\mathbf{q}[N_{k+1}] - \mathbf{q}[N_k]\|_2 \gg \Delta$, $\forall k = 1, 2, \dots, K-1$. If two adjacent target locations are close, i.e., $\|\mathbf{q}[N_{k+1}] - \mathbf{q}[N_k]\|_2 \approx \Delta$, they can be combined as a single target location.

Denoting the time slot that the UAV flies in the n -th line segment by $t[n]$, we thus have $T_k = \sum_{n=1}^{\hat{N}} t[n]$, $\forall k = 1, 2, \dots, K$. Letting $\mathbf{v}[n]$ denote the velocity of the UAV at the n -th waypoint, the velocity in $t[n]$ can thus be approximated as $\frac{\mathbf{v}[n+1] + \mathbf{v}[n]}{2}$. Therefore, the data acquisition rate in $t[n]$ is approximated as $\dot{\zeta}[n] = \Theta(\frac{\|\mathbf{v}[n+1]\|_2 + \|\mathbf{v}[n]\|_2}{2})$. Hence, letting $\mathcal{N} \triangleq \{1, 2, \dots, \hat{N}\}$, (10) and (12) can be respectively expressed as

$$\mathbf{q}[n+1] - \mathbf{q}[n] = \frac{\mathbf{v}[n+1] + \mathbf{v}[n]}{2} t[n], \quad \forall n \in \mathcal{N}, \quad (15)$$

$$\mathbf{a}[n] = \frac{\mathbf{v}[n+1] - \mathbf{v}[n]}{t[n]}, \quad \forall n \in \mathcal{N}, \quad (16)$$

where $\mathbf{a}[n]$ denotes the UAV acceleration in $t[n]$. Besides, we denote the transmission power $p(t)$ and CPU frequency $f(t)$ in $t[n]$ by $p[n]$ and $f[n]$, respectively. Therefore, the energy consumption can be rewritten as

$$E^p = \sum_{n=1}^{\hat{N}} \left[c_1 \|\mathbf{v}[n]\|_2^3 + \frac{c_2}{\|\mathbf{v}[n]\|_2} \left(1 + \frac{\|\mathbf{a}[n]\|_2^2}{g^2} \right) \right] t[n],$$

$$E^c = \sum_{n=1}^{\hat{N}} \eta L f[n]^3 t[n],$$

$$E^o = \sum_{n=1}^{\hat{N}} (P_0 + c_p p[n]) t[n].$$

Moreover, we consider that the channel in $t[n]$ is constant with $\mathbf{q}[n]$ and $p[n]$. Hence, the channel capacity is then rewritten as

$$\begin{aligned}
 R[n] &= B \log_2 \left(1 + \frac{\gamma_0[n]}{H^2 + \|\mathbf{q}[n] - \mathbf{Q}_{BS}\|_2^2} \right) \\
 &= B \log_2 \left(1 + \frac{p[n]\beta_0}{\sigma^2 (H^2 + \|\mathbf{q}[n] - \mathbf{Q}_{BS}\|_2^2)} \right),
 \end{aligned}$$

where $\gamma_0[n]$ denotes the SNR at the distance of 1 m in $t[n]$.

For notation convenience, let $\mathbf{p} \triangleq \{p[1] \ p[2] \ \dots \ p[\hat{N}]\}^T \triangleq \{p[n]\}$, $\mathbf{q} \triangleq \{\mathbf{q}[n]\}$, $\mathbf{a} \triangleq \{\mathbf{a}[n]\}$, $\mathbf{v} \triangleq \{\mathbf{v}[n]\}$, $\mathbf{f} \triangleq \{f[n]\}$, $\mathbf{t} \triangleq \{t[n]\}$. Note that both \mathbf{q} and \mathbf{a} can be uniquely determined by \mathbf{v} and \mathbf{t} . Therefore, problem (P-1) can be reformulated as the discrete form:

$$\begin{aligned}
 & \text{(P-2)} \quad \min_{\mathbf{v}, \mathbf{t}, \mathbf{f}, \mathbf{p}} E^c + E^p + E^o \\
 & \text{s.t.} \quad f[n]/\eta + R[n] \geq \dot{\zeta}[n], \quad \forall n \in \mathcal{N}, \quad (17)
 \end{aligned}$$

$$0 \leq p[n] \leq P, \quad \forall n \in \mathcal{N}, \quad (18)$$

$$0 \leq f[n] \leq F, \quad \forall n \in \mathcal{N}, \quad (19)$$

$$\begin{aligned}
 & \mathbf{q}[n+1] - \mathbf{q}[n] \\
 &= \frac{\mathbf{v}[n+1] + \mathbf{v}[n]}{2} t[n], \quad \forall n \in \mathcal{N}, \quad (20)
 \end{aligned}$$

$$\mathbf{a}[n] = \frac{\mathbf{v}[n+1] - \mathbf{v}[n]}{t[n]}, \quad \forall n \in \mathcal{N}, \quad (21)$$

$$V_{\min} \leq \|\mathbf{v}[n]\|_2 \leq V_{\max}, \quad \forall n \in \mathcal{N}, \quad (22)$$

$$\|\mathbf{a}[n]\|_2 \leq a_{max}, \forall n \in \mathcal{N}, \quad (23)$$

$$\|\mathbf{q}[n+1] - \mathbf{q}[n]\|_2 \leq \Delta, \forall n \in \mathcal{N}, \quad (24)$$

$$\|\mathbf{q}[N_k] - \mathbf{Q}_k\|_2 \leq D_k, \forall k = 1, 2, \dots, K. \quad (25)$$

One can observe that problem (P-2) is not convex due to the non-convex constraints (17), (20)–(25) and non-convex objective function, where many variables are coupled with each other. Therefore, problem (P-2) is challenging to solve. To tackle this highly complex problem, we propose an efficient three-stage iterative algorithm based on the block coordinates descent (BCD) technique. Specifically, at the first stage, UAV velocity \mathbf{v} is optimized with given $\{\mathbf{t}, \mathbf{f}, \mathbf{p}\}$; at the next stage, we optimize time duration \mathbf{t} with given $\{\mathbf{v}, \mathbf{p}, \mathbf{f}\}$; at the last stage, for given $\{\mathbf{t}, \mathbf{v}\}$, the task allocation related variables, i.e., transmit power \mathbf{p} and CPU frequency \mathbf{f} , are optimized simultaneously by solving a convex problem. We optimize the three sub-problems alternatively until the solution converges.

A. UAV Velocity Optimization

For any given $\{\mathbf{t}, \mathbf{f}, \mathbf{p}\}$, \mathbf{q} and \mathbf{a} can be uniquely determined by \mathbf{v} , hence problem (P-2) is reduced to

$$\begin{aligned} (\text{P-3}) \quad & \min_{\mathbf{v}} \quad E^p \\ \text{s.t.} \quad & (17), (20)–(25). \end{aligned}$$

It can be shown that E^p is not convex with respect to \mathbf{v} . Therefore, we introduce slack variables $\tau \triangleq \{\tau[n]\}$ and reformulate problem (P-3) as

$$\begin{aligned} (\text{P-3.1}) \quad & \min_{\tau, \mathbf{v}} \sum_{n=1}^N \left[c_1 \|\mathbf{v}[n]\|_2^3 + \frac{c_2}{\tau[n]} \left(1 + \frac{\|\mathbf{a}[n]\|_2^2}{g^2} \right) \right] t[n] \\ \text{s.t.} \quad & (17), (20)–(21), (23)–(25), \end{aligned}$$

$$\|\mathbf{v}[n]\|_2 \leq V_{max}, \forall n \in \mathcal{N}, \quad (26)$$

$$\tau[n]^2 \leq \|\mathbf{v}[n]\|_2^2, \forall n \in \mathcal{N}, \quad (27)$$

$$V_{min} \leq \tau[n], \forall n \in \mathcal{N}. \quad (28)$$

One can derive that (27) is met with equality at the optimal solution to problem (P-3.1), since otherwise $\tau[n]$ can always be increased to decrease the objective value with all the other constraints being still satisfied. Therefore, problem (P-3.1) is equivalent to problem (P-3). It can be verified that the objective function of problem (P-3.1) is convex with respect to $\{\tau, \mathbf{v}\}$. However, with the existence of non-convex constraints (17) and (27), problem (P-3.1) is still non-convex. Hence, we utilize the successive convex approximation (SCA) technique to tackle such non-convexity.

With SCA, instead of solving the non-convex problem (P-3.1) directly, a convex optimization problem is performed at each iteration by local approximation. Note that $\|\mathbf{v}[n]\|_2^2$ is a differentiable convex function with respect to $\mathbf{v}[n]$. Besides, it is known that the first-order Taylor expansion of a differentiable convex function is its global under-estimator at a given local point [49]. Therefore, at iteration i , the convex function $\|\mathbf{v}[n]\|_2^2$

in constraint (27) is lower bounded by its first-order Taylor expansion at a given local point $\mathbf{v}[n]^{(i)}$:

$$\|\mathbf{v}[n]\|_2^2 \geq \left\| \mathbf{v}[n]^{(i)} \right\|_2^2 + 2(\mathbf{v}[n]^{(i)})^T (\mathbf{v}[n] - \mathbf{v}[n]^{(i)}). \quad (29)$$

For constraint (17), it can be shown that $R[n]$ is differentiable and convex with respect to the term $\|\mathbf{q}[n] - \mathbf{Q}_{BS}\|_2^2$. Similar as in [45], we can obtain the lower bound of $R[n]$ with a given point $\mathbf{q}[n]^{(i)} = \mathbf{q}[1] + \sum_{m=2}^n \frac{\mathbf{v}[m]^{(i)} + \mathbf{v}[m-1]^{(i)}}{2} t[m-1]$ at iteration i ,

$$\begin{aligned} R[n] \geq B \left[M^{(i)} - F^{(i)} \left(\|\mathbf{q}[n] - \mathbf{Q}_{BS}\|_2^2 \right. \right. \\ \left. \left. - \left\| \mathbf{q}[n]^{(i)} - \mathbf{Q}_{BS} \right\|_2^2 \right) \right] \triangleq \xi(\mathbf{q}[n])^{(i)}, \end{aligned} \quad (30)$$

where

$$M^{(i)} = \log_2 \left(1 + \frac{\gamma_0[n]}{H^2 + \|\mathbf{q}[n]^{(i)} - \mathbf{Q}_{BS}\|_2^2} \right),$$

and

$$F^{(i)} = \frac{\gamma_0[n](\log_2 e)(H^2 + \|\mathbf{q}[n]^{(i)} - \mathbf{Q}_{BS}\|_2^2)^{-1}}{(H^2 + \gamma_0[n] + \|\mathbf{q}[n]^{(i)} - \mathbf{Q}_{BS}\|_2^2)}.$$

Note that function $\xi(\mathbf{q}[n])^{(i)}$ is concave with respect to $\mathbf{q}[n]$, and $\mathbf{q}[n] - \mathbf{q}_1, \forall n = 2, \dots, N_K$, is a conic combination of the elements of \mathbf{v} under given \mathbf{t} as shown in (20). Therefore, $\xi(\mathbf{q}[n])^{(i)}$ is concave with respect to \mathbf{v} under given \mathbf{t} . As a result, by replacing $R[n]$ and $\|\mathbf{v}[n]\|_2^2$ with their local lower bounds, at iteration i , we have the following convex problem for given local points $\{\mathbf{v}[n]^{(i)}\}$,

$$(\text{P-3.2}) \quad \min_{\tau, \mathbf{v}} \sum_{n=1}^{\hat{N}} \left[c_1 \|\mathbf{v}[n]\|_2^3 + \frac{c_2}{\tau[n]} \left(1 + \frac{\|\mathbf{a}[n]\|_2^2}{g^2} \right) \right] t[n]$$

$$\text{s.t.} \quad (20)–(21), (23)–(26), (28),$$

$$\xi(\mathbf{q}[n])^{(i)} + f[n]/\eta \geq \zeta[n], \forall n \in \mathcal{N}, \quad (31)$$

$$\begin{aligned} & \left\| \mathbf{v}[n]^{(i)} \right\|_2^2 + 2(\mathbf{v}[n]^{(i)})^T (\mathbf{v}[n] - \mathbf{v}[n]^{(i)}) \\ & \geq \tau[n]^2, \forall n \in \mathcal{N}. \end{aligned} \quad (32)$$

The standard convex optimization methods, such as the interior-point method [49], can be utilized to solve problem (P-3.2). The SCA-based algorithm to solve the UAV velocity optimization problem is summarized in Algorithm 1.

Note that the objective value of problem (P-3.2) is monotonically non-increasing after each iteration in Algorithm 1. Furthermore, the obtained solution is guaranteed to satisfy the Karush-Kuhn-Tucker (KKT) conditions of problem (P-3) [50]. Since a convex optimization problem is solved at each iteration, Algorithm 1 has a polynomial complexity in the worst case [49].

Algorithm 1: SCA-Based Algorithm to Solve Problem (P-3).

- 1: Input: $\{\mathbf{v}[n]^{(0)}\}$. Let $i=0$.
 - 2: **repeat**
 - 3: Solving problem (P-3.2) with given $\{\mathbf{v}[n]^{(i)}\}$, and obtain $\{\mathbf{v}[n]^{(i+1)}\}$.
 - 4: Update $i = i + 1$.
 - 5: **until** The fractional decrease of the objective value of problem (P-3.2) is below a prescribed threshold ϵ .
 - 6: Output: $\{\mathbf{v}[n]^{(i)}\}$.
-

B. Time Duration Optimization

Next, we optimize the time duration with given $\{\mathbf{v}, \mathbf{f}, \mathbf{p}\}$. Since here \mathbf{q} and \mathbf{a} can be uniquely determined by \mathbf{t} , the subproblem is given by

$$(P-4) \quad \min_{\mathbf{t}} \quad E^c + E^p + E^o$$

$$\text{s.t.} \quad (17), (20)-(21), (23)-(25).$$

With given $\{\mathbf{v}, \mathbf{f}, \mathbf{p}\}$, constraint (17) can be rewritten as a quadratic constraint form:

$$\|\mathbf{q}[n] - \mathbf{Q}_{BS}\|_2^2 \leq \frac{p[n]\beta_0}{\sigma^2} \left(2^{\frac{\zeta[n]-f[n]/\eta}{B}} - 1\right)^{-1} - H^2. \quad (33)$$

Note that (33) is convex with respect to $\mathbf{q}[n]$ and (20) shows that $\mathbf{q}[n], \forall n = 2, \dots, N_K$, is an affine function of \mathbf{t} under given \mathbf{v} . Hence, (33) is convex with respect to \mathbf{t} for any given \mathbf{v} . By replacing (17) with (33), we can reformulate problem (P-4) in an equivalent form as

$$(P-4.1) \quad \min_{\mathbf{t}} \quad E^c + E^p + E^o$$

$$\text{s.t.} \quad (20)-(21), (23)-(25), (33).$$

It can be verified that problem (P-4.1) is a convex optimization problem, which can be solved by using the standard convex optimization method (similar to problem (P-3.2)). Since the objective function of problem (P-4.1) is monotonically increasing with respect to \mathbf{t} , the optimal solution must lie on the boundary of the feasible region.

C. Resource Allocation Optimization

Finally, with given UAV velocity \mathbf{v} and time duration \mathbf{t} , we optimize the resource allocation, which comprises the transmission power \mathbf{p} and CPU frequency \mathbf{f} . The subproblem is given by

$$(P-5) \quad \min_{\mathbf{f}, \mathbf{p}} \quad E^c + E^o$$

$$\text{s.t.} \quad (17)-(19).$$

First of all, it is noted that the equality of constraint (17) must be held at the optimal solution. Suppose on the contrary, if (17) does not reach equality at the optimal solution, one can always decrease $p[n]$ or $f[n]$ to obtain a strictly smaller objective value while all other constraints are still satisfied. To obtain a more tractable problem form, we define a variable $\lambda[n]$ that indicates the ratio of local computing data to the total data generated

in time slot $t[n]$. Therefore, the local computing rate can be reformulated as $f[n]/\eta = \lambda[n]\dot{\zeta}[n]$, and the data offloading rate can be reformulated as $R[n] = (1 - \lambda[n])\dot{\zeta}[n]$. We can then rewrite constraint (17) as

$$p[n] = \frac{\sigma^2 \left(2^{\frac{(1-\lambda[n])\dot{\zeta}[n]}{B}} - 1\right)}{h[n]}, \quad \forall n \in \mathcal{N}, \quad (34)$$

$$f[n] = \eta\lambda[n]\dot{\zeta}[n], \quad \forall n \in \mathcal{N}. \quad (35)$$

Therefore, constraints (18) and (19) become as

$$0 \leq \frac{\sigma^2 \left(2^{\frac{(1-\lambda[n])\dot{\zeta}[n]}{B}} - 1\right)}{h[n]} \leq P, \quad \forall n \in \mathcal{N}, \quad (36)$$

$$0 \leq \eta\lambda[n]\dot{\zeta}[n] \leq F \quad \forall n \in \mathcal{N},$$

$$0 \leq \lambda[n] \leq 1, \quad \forall n \in \mathcal{N}. \quad (37)$$

As a result, by replacing $f[n]$ and $p[n]$ with $\lambda[n]$, we can reduce the number of variables in problem (P-5) to one. Letting $\Lambda \triangleq \{\lambda[n]\}$, we obtain an equivalent formulation of problem (P-5) after some simplifications

$$(P-5.1) \quad \min_{\Lambda} \quad E^c + E^o$$

$$\text{s.t.} \quad \check{\lambda}[n] \leq \lambda[n] \leq \hat{\lambda}[n], \quad \forall n \in \mathcal{N}, \quad (38)$$

where

$$E^c = \sum_{n=1}^{\hat{N}} \left(\eta\lambda[n]\dot{\zeta}[n]\right)^3 Lt[n],$$

$$E^o = \sum_{n=1}^{\hat{N}} \frac{\sigma^2 \left(2^{\frac{(1-\lambda[n])\dot{\zeta}[n]}{B}} - 1\right)}{h[n]} t[n],$$

and

$$\check{\lambda}[n] = \max \left(1 - \frac{B \log_2 \left(\frac{Ph[n]}{\sigma^2} + 1\right)}{\dot{\zeta}[n]}, 0\right),$$

$$\hat{\lambda}[n] = \min \left(\frac{F}{\eta\dot{\zeta}[n]}, 1\right).$$

It can be shown that problem (P-5.1) is a standard convex optimization problem.

Lemma 1: The optimal solution $\{p[n]^*, f[n]^*\}$ to problem (P-5) are given by

$$\lambda[n]^* = \min \left(\hat{\lambda}[n], \max(\lambda_0[n], \check{\lambda}[n])\right), \quad \forall n \in \mathcal{N}, \quad (39)$$

$$p[n]^* = \frac{\sigma^2 \left(2^{\frac{(1-\lambda[n]^*)\dot{\zeta}[n]}{B}} - 1\right)}{h[n]}, \quad \forall n \in \mathcal{N}, \quad (40)$$

$$f[n]^* = \eta\lambda[n]^*\dot{\zeta}[n], \quad \forall n \in \mathcal{N}, \quad (41)$$

where $\lambda_0[n]$ is the root of the equation

$$3L\eta^3\dot{\zeta}[n]^3 t[n]\lambda[n]^2$$

$$- \frac{t[n]\dot{\zeta}[n]\sigma^2}{Bh[n]} 2^{\frac{(1-\lambda[n])\dot{\zeta}[n]}{B}} \ln 2 = 0, \quad \forall n \in \mathcal{N}. \quad (42)$$

Proof: See Appendix A. \square

Algorithm 2: Overall Algorithm to Solve Problem (P-2).

-
- 1: Input: $\{\mathbf{v}^{(0)}, \mathbf{t}^{(0)}, \mathbf{f}^{(0)}, \mathbf{p}^{(0)}\}$. Let $j=0$.
 - 2: **repeat**
 - 3: Solve problem (P-3.1) with given $\{\mathbf{v}^{(j)}, \mathbf{t}^{(j)}, \mathbf{f}^{(j)}, \mathbf{p}^{(j)}\}$ by Algorithm 1, and obtain the optimal solution $\{\mathbf{v}^{(j+1)}\}$.
 - 4: Solve convex problem (P-4.1) with given $\{\mathbf{v}^{(j+1)}, \mathbf{f}^{(j)}, \mathbf{p}^{(j)}\}$, and obtain the optimal solution $\{\mathbf{t}^{(j+1)}\}$.
 - 5: Solve convex problem (P-5.1) with given $\{\mathbf{v}^{(j+1)}, \mathbf{t}^{(j+1)}\}$, and obtain the closed-form optimal solution $\{\mathbf{f}^{(j+1)}, \mathbf{p}^{(j+1)}\}$.
 - 6: Update $j = j + 1$.
 - 7: **until** The fractional decrease of the objective value of problem (P-2) is below a prescribed threshold ϵ .
 - 8: Output: $\{\mathbf{v}^{(j)}, \mathbf{t}^{(j)}, \mathbf{f}^{(j)}, \mathbf{p}^{(j)}\}$.
-

D. Overall Algorithm and Convergence

Based on the above discussion, the overall three-stage iterative algorithm for problem (P-2) is summarized in Algorithm 2, which solves three subproblems (P-3.1), (P-4.1) and (P-5.1) alternately until the objective value of problem (P-2) converges to a given accuracy. The initialization procedure is discussed in the next subsection.

It is important to note that in the classical BCD method, we must optimize every subproblem exactly in order to guarantee the convergence. However, in this work, problem (P-3.1) is approximately solved by applying SCA. In what follows, we outline the convergence analysis for our proposed Algorithm 2. Denote $E(\mathbf{v}, \mathbf{t}, \mathbf{f}, \mathbf{p})$ as the objective value of problem (P-2) and $\tilde{E}(\mathbf{v}, \mathbf{t}, \mathbf{f}, \mathbf{p})$ as the objective value of the approximate problem (P-3.2) plus the E^o and E^c . We thus have,

$$\begin{aligned}
E(\mathbf{v}^{(j)}, \mathbf{t}^{(j)}, \mathbf{f}^{(j)}, \mathbf{p}^{(j)}) &\stackrel{(a)}{=} \tilde{E}(\mathbf{v}^{(j)}, \mathbf{t}^{(j)}, \mathbf{f}^{(j)}, \mathbf{p}^{(j)}) \\
&\stackrel{(b)}{\geq} \tilde{E}(\mathbf{v}^{(j+1)}, \mathbf{t}^{(j)}, \mathbf{f}^{(j)}, \mathbf{p}^{(j)}) \stackrel{(c)}{=} E(\mathbf{v}^{(j+1)}, \mathbf{t}^{(j)}, \mathbf{f}^{(j)}, \mathbf{p}^{(j)}) \\
&\stackrel{(d)}{\geq} E(\mathbf{v}^{(j+1)}, \mathbf{t}^{(j+1)}, \mathbf{f}^{(j)}, \mathbf{p}^{(j)}) \stackrel{(e)}{\geq} E(\mathbf{v}^{(j+1)}, \mathbf{t}^{(j+1)}, \mathbf{f}^{(j+1)}, \mathbf{p}^{(j+1)}),
\end{aligned}$$

where (a) and (c) hold since the first-order Taylor expansions in problems (P-3.2) and (P-3) are tight at the given local points $\mathbf{v}^{(j)}$ and $\mathbf{v}^{(j+1)}$, respectively; (b) holds since the optimal velocity $\mathbf{v}^{(j+1)}$ is obtained by Algorithm 1 with fixed $\{\mathbf{t}^{(j)}, \mathbf{f}^{(j)}, \mathbf{p}^{(j)}\}$; (d) and (e) hold since problem (P-4.1) and problem (P-5.1) are optimally solved respectively. Therefore, we have $E(\mathbf{v}^{(j)}, \mathbf{t}^{(j)}, \mathbf{f}^{(j)}, \mathbf{p}^{(j)}) \geq E(\mathbf{v}^{(j+1)}, \mathbf{t}^{(j+1)}, \mathbf{f}^{(j+1)}, \mathbf{p}^{(j+1)})$, which indicates that the objective value of problem (P-2) is non-increasing over each iteration of Algorithm 2. Since $E(\mathbf{v}, \mathbf{t}, \mathbf{f}, \mathbf{p})$ is lower bounded by a finite value, Algorithm 2 is guaranteed to converge to a locally optimal solution of problem (P-2).

E. Initialization

It is known that both BCD and SCA techniques depend much on the initial solution in general. To promote convergence and improve the optimality of converged results, an efficient initial design is needed.

In the simple case with two target locations, the UAV only needs to traverse the initial and final locations, where the trajectory initialization can be simply set as a circle or a straight-line path with a constant UAV speed as in most existing works. Nevertheless, in our multiple target locations problem, a straight-forward initialization, such as setting straight lines between every two adjacent visitation locations as the initial path, is inefficient for the algorithms and directly penalizes the final system performance. Specifically, 1) For a $D_k > 0$, the UAV does not need to traverse above the target location \mathbf{Q}_k in general. Otherwise, it leads to unnecessary flying distances, energy and MCT consumption; 2) Generally, a rough trajectory with sharpening turnings requires extremely high acceleration magnitudes, which brings huge energy consumption to the system; 3) Considering the kinematic constraints (22)-(23), a rough initial trajectory tends to be infeasible for the problem, which results that the algorithms cannot be executed. To this end, we propose the following systematic and generic method with four steps, which can obtain an efficient initial design.

- 1) In general, minimizing the flying distance can reduce the UAV propulsion energy consumption. Therefore, we firstly minimize the total flying distance in the absence of other constraints. The problem can be formulated as

$$\begin{aligned}
(P-6) \quad &\min_{\mathbf{q}[n]} \sum_{n=1}^{\hat{N}} \|\mathbf{q}[n+1] - \mathbf{q}[n]\|_2 \\
&\text{s.t.} \quad (25).
\end{aligned}$$

It has been proved that the optimal solution to problem (P-6) is only composed of line segments, and problem (P-6) equals to finding the optimal set of visitation locations denoted by $\{\mathbf{q}_k^*\}$ in the disks [44], as shown in Fig. 2(a).

- 2) Next, we focus on the smoothing of the solution obtained above. As mentioned before, a rough trajectory is energy-inefficient or even unflyable for fixed-wing UAVs. To avoid the sharp turning at the intersection of two line segments, here circle arcs are served as the transfer functions to connect the line segments³. We specify circle centered at the extension of line segment between optimal visitation location \mathbf{q}_k^* and target location \mathbf{Q}_k with turning radius $R_{ini} \geq \frac{V_{min}^2}{a_{max}}$, where \mathbf{o}_k denotes the circle center and $\frac{V_{min}^2}{a_{max}}$ is the approximated minimum turn radius. After that, by modifying the previous line segments with Dubins curves [52], a smooth trajectory can be obtained as shown in Fig. 2(b).

³Note that the trajectory composed of line segments and circle arcs only possesses first-order derivative continuity, whose curvature is not continuous. A smoother trajectory can be obtained by high-order polynomial function such as Bézier curve [51].

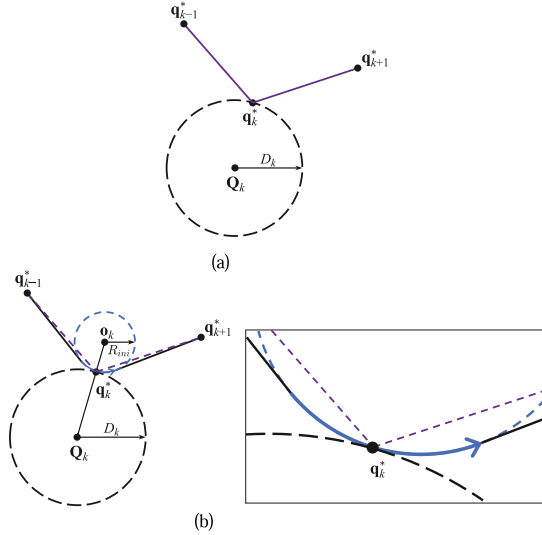


Fig. 2. An illustration of the trajectory initialization. (a) Trajectory obtained by problem (P-6). (b) Smooth trajectory with Dubins curve.

- 3) Until now, the speed still needs to be specified. To make the problem more tractable, we use the trapezoidal move profile,⁴ where the UAV motion consists of uniform motion, uniform variable motion, and uniform circular motion. The default speed setting of uniform motion is the power-minimum speed (PMS) $V_{pm} \triangleq (c_2/3c_1)^{1/4}$ [45] to reduce the propulsion energy consumption. The speeds of the other two motions are set to be greater than or equal to the minimum speed V_{min} , and the acceleration magnitude of the uniform variable motion is set to be less than or equal to a_{max} . Therefore, the obtained trajectory is guaranteed to satisfy the kinematic constraints (22), (23). Furthermore, since now the exact mathematic expressions of the entire initial trajectory can be obtained, we can easily compute its corresponding discretization form.
- 4) However, the obtained trajectory from the first three steps may not satisfy the constraints (17)–(19), i.e., it may not be feasible for the problem (P-5). Nonetheless, if the data acquisition rate is greater than the total processing ability, we can always set a lower UAV speed, and thus further decrease the data acquisition rate. Therefore, we can eventually obtain a feasible initial trajectory and with that, we can also obtain the initial $\{f, p\}$ from solving problem (P-5).

IV. AN ALTERNATIVE CASE: MISSION COMPLETION TIME MINIMIZATION PROBLEM

Under some application scenarios, people may care the MCT more than the UAV energy consumption. In this section, we study the MCT minimization problem without considering the energy limitation, i.e., assuming that the UAV's battery capacity is large enough. Therefore, regarding the problem formulation, we do not choose to optimize f and p , and they are set as the

⁴For simplicity, we do not consider a smoother speed initialization such as S-curve motion.

maximum allowable value. Besides, since the energy consumption is not the main concern, we expect the UAV flies as fast as possible (under constraints (17) and (22)) to reduce the MCT. Hence, the MCT minimization problem can be formulated as

$$(P-7) \quad \min_{\mathbf{v}, \mathbf{t}} \quad \sum_{n=1}^{\hat{N}} t[n] + \delta \sum_{n=1}^{\hat{N}+1} (\|\mathbf{v}[n]\|_2 - V_{max})^2$$

s.t. (17), (20)–(25),

where the second term in the objective function is to keep the speed closer to V_{max} and $\delta > 0$ is a scaling factor.

Observing that problems (P-7) and (P-2) have similar structures, we thus employ the similar BCD approach to solve problem (P-7).

At the first stage, we optimize \mathbf{t} with given \mathbf{v} . The subproblem is formulated as

$$(P-8) \quad \min_{\mathbf{t}} \quad \sum_{n=1}^{\hat{N}} t[n]$$

s.t. (17), (20)–(21), (23)–(25).

Similar to problem (P-4), it can be shown that problem (P-8) is a convex optimization problem with the optimal solution lying on the feasible region boundary, which can be solved efficiently by the standard algorithms.

At the second stage, we aim to maximize the UAV speed with given \mathbf{t} . Hence, we have the subproblem as

$$(P-9) \quad \min_{\mathbf{v}} \quad \delta \sum_{n=1}^{\hat{N}+1} (\|\mathbf{v}[n]\|_2 - V_{max})^2$$

s.t. (17), (20)–(25).

Due to the similar structure to that of problem (P-5), we can obtain an approximate solution of problem (P-9) by means of SCA as used in problem (P-5), which converges to at least a locally optimal solution. Specifically, the channel capacity $R[n]$ and the speed $\|\mathbf{v}[n]\|_2$ are respectively replaced by their lower bounds at given local points in each iteration. The details are omitted for brevity.

Furthermore, because that the objective function of problem (P-7) has a finite lower bound, the overall BCD algorithm for problem (P-7) is guaranteed to converge as discussed before. The algorithm details follow similar steps of Algorithm 2, which are summarized as in Algorithm 3.

Note that problem (P-7) is for MCT, if one is interested in calculating the UAV energy consumption under the obtained optimal solution $\{\mathbf{v}^*, \mathbf{t}^*\}$ from problem (P-7), it is required to solve problem (P-5) with given $\{\mathbf{v}^*, \mathbf{t}^*\}$.

A. Implementation

Our system can be implemented by an end user as follows:

- 1) Determining a feasible data acquisition model based on the practical mission demands;
- 2) Setting the key parameters, such as the target locations, MEC server location, visitation order, flying altitude, etc;

Algorithm 3: Overall Algorithm to Solve Problem (P-7).

-
- 1: Initialization: $\{\mathbf{v}^{(0)}, \mathbf{t}^{(0)}\}$. Let $j=0$.
 - 2: **repeat**
 - 3: Solve convex problem (P-8) with given $\{\mathbf{v}^{(j)}\}$, and obtain the optimal solution $\{\mathbf{t}^{(j+1)}\}$.
 - 4: Solve problem (P-9) with given $\{\mathbf{t}^{(j+1)}\}$ by SCA, and obtain the optimal solution $\{\mathbf{v}^{(j+1)}\}$.
 - 5: Update $j = j + 1$.
 - 6: **until** The fractional decrease of the objective value of problem (P-7) is below a prescribed threshold ϵ .
 - 7: Output: $\{\mathbf{v}^{(j)}, \mathbf{t}^{(j)}\}$.
-

- 3) Computing the UAV trajectory and resource allocation scheme by our proposed Algorithm 2 or Algorithm 3 based on demands. Then inputting the results into the UAV;
- 4) The mission starts.

V. SIMULATION RESULTS

In this section, numerical results are provided to illustrate the performance of our proposed design and algorithms. Namely, we have proposed the following two algorithms:

- 1) *Energy min (EM)*: The proposed energy minimization Algorithm 2 for problem (P-2);
- 2) *Time min (TM)*: The proposed MCT Algorithm 3 for problem (P-7).

To validate the effectiveness of our proposed algorithms, the following benchmark methods are involved to compare with the above two algorithms:

- 1) *Without offloading (WO)*: All the acquired data are processed locally without offloading to the MEC server. When solving problem (P-5), we set $\Lambda^* = \mathbf{1}$, thus having $p[n]^* = 0$, and $f[n]^* = \eta\zeta[n]$;
- 2) *All offloaded (AO)*: All the acquired data are offloaded to the server. When solving problem (P-5), we set $\Lambda^* = \mathbf{0}$, thus having $p[n]^* = \frac{\sigma^2(2^{\frac{\zeta[n]}{B}} - 1)}{h[n]}$, and $f[n]^* = 0$. On this basis, we use *AO-energy* and *AO-time* to denote the benchmarks obtained by solving problems (P-2) and (P-7) with AO method, respectively;
- 3) *Fixed power (FP)*: With given \mathbf{p} , problem (P-2) can be optimized by alternatively solving two subproblems only. The first subproblem is

$$(P-10) \quad \min_{\mathbf{v}, \mathbf{f}} \quad E^c + E^p$$

$$\text{s.t.} \quad (17), (19)-(25),$$

which can be solved by SCA techniques as mentioned before. The second subproblem is problem (P-4). In the simulation, the transmission power is set as $\mathbf{p} = 2 \text{ W}$;

- 4) *Propulsion First (PF)*: For this scheme, we firstly set and fix $\{\mathbf{f}, \mathbf{p}\}$ as their maximum value, then problem (P-2) is reduced to the propulsion energy consumption minimization problem with respect to $\{\mathbf{v}, \mathbf{t}\}$, which can be further decomposed into only two subproblems (P-3) and (P-4) by BCD method. Finally, we substitute the obtained $\{\mathbf{v}^*, \mathbf{t}^*\}$

into problem (P-5) to obtain the total energy consumption for the UAV.

In the simulation, the specific data acquisition rate model is set as

$$\dot{\zeta}[n] = \Theta\left(\frac{\|\mathbf{v}[n+1]\|_2 + \|\mathbf{v}[n]\|_2}{2}\right)$$

$$= \alpha \left(\frac{\|\mathbf{v}[n+1]\|_2 + \|\mathbf{v}[n]\|_2}{2} + \rho \right), \forall n \in \mathcal{N}, \quad (43)$$

where α is data generation coefficient (DGC) in bit/m to measure linear increase of the data acquisition rate with the UAV speed, and ρ is a constant in m/s that measures the data acquisition rate when UAV is static. Under the premise of satisfying the property of $\Theta(\cdot)$ in (3), the linear function (43) is utilized in the simulation for simplicity. However, one can choose a more complicated function based on the practical mission demands, while maintaining the feasibility.

Unless stated, the default simulation parameters are shown in Table I.

Fig. 3 depicts the benefits brought by our proposed MEC-assisted design against the benchmark scheme (i.e., WO), where the maximum DGC is obtained by checking whether the initial solution is feasible or not. It is observed that, with our proposed MEC-assisted design, 1) The real-time data acquisition and processing ability of the UAV system is greatly enhanced, since the maximum allowable DGC is much larger than that of the benchmark scheme; 2) The energy consumption of UAV is vastly reduced; 3) The MCT is significantly cut down. In other words, with the assistance of MEC, UAV is able to timely acquire and process a huge amount of data, saving enormous energy and MCT, which confirms the effectiveness of our design.

Fig. 4 indicates the UAV trajectories information obtained by different schemes, for small and large DGCs, respectively. The *Initial-path* is obtained from Section III-E. Wherein, Figs. 4(a) and (b) show paths for different DGC α , and Figs. 4(c) and (d) show the corresponding speeds versus time instant. It is known that the UAV propulsion power decreases when the UAV speed approaches the PMS V_{pm} in general [45], and thus both small and large speeds are relatively propulsion power-consuming. Hence, a *PMS* line is applied here as a reference for propulsion power. Firstly, it is observed from Figs. 4(a) and (c) that, for small α , trajectories tendencies of EM, AO-energy, FP, and PF schemes are very similar. However, for large α , the trajectories of these four schemes can be divided into two significantly different groups from the observation from Figs. 4(b) and (d). This is because that when α is small, the amount of data that needs to be processed is thus relatively small. With a large feasible region, AO-energy and FP schemes are able to obtain the trajectories that are close to the EM trajectory. However, for large α , they can merely obtain energy-inefficient trajectories, where the UAVs need to fly as close as possible to BS to enjoy better communication channels and slow down to guarantee the real-time processing. Such trajectories can lead to longer flying distances and propulsion power-consuming low speeds, which further cause large energy and MCT consumption. It can be observed from Fig. 4(c) that, except for the WO speed curve, the other five speed curves are W-shaped. This is because the

TABLE I
DEFAULT PARAMETER SETUP

Parameter	Value	Parameter	Value	Parameter	Value	Parameter	Value
H	20 m	β_0	-50 dB [45]	σ^2	-110 dBm [45]	R_{ini}	20 m
η	500	F	4 GHz	L	10^{-28}	c_1	$9.26 * 10^{-4}$ [45]
P	2 W	c_p	18 [47]	P_0	0.4 W [47]	c_2	2250 [45]
V_{min}	5 m/s [45]	V_{max}	50 m/s	a_{max}	5 m/s ²	Δ	10 m
g	9.8 m/s ²	\mathbf{Q}_1	(100,100)	\mathbf{Q}_2	(500,0)	\mathbf{Q}_{BS}	(600,400)
\mathbf{Q}_3	(800,500)	\mathbf{Q}_4	(1200,300)	D_1, D_4	0 m	D_2, D_3	50 m
ρ	10 m/s	B	3 MHz	\bar{N}	301	N_2	90
N_3	210	ϵ	0.1%	δ	1		

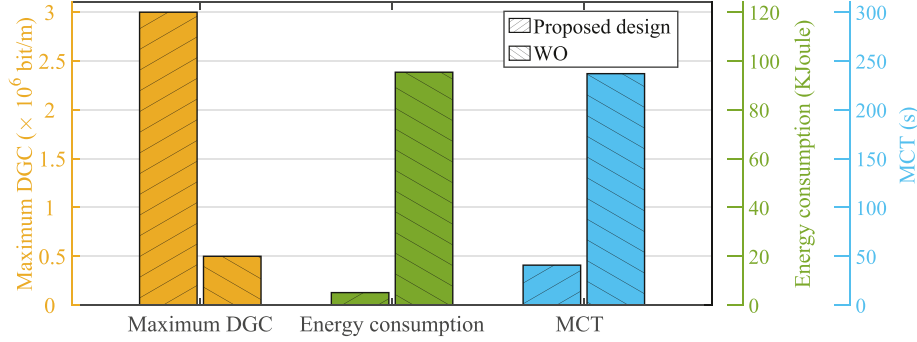


Fig. 3. System gain, where the energy consumption and MCT are obtained under $\alpha = 0.5 \times 10^6$ bit/m.

UAV needs to slow down at the turn points to obtain a small turn radius, where the turn speed of TM scheme is lower than the others due to the smaller turn radius as shown in Fig. 4(a). In contrast, the speed of the WO scheme tends to maintain a value around V_{min} due to the limited on-board computation resources, which causes massive energy and MCT consumption as shown in Fig. 3. Besides, it is observed from Fig. 4(a) that the path of WO is more straight than the other paths. This is reasonable since the UAV does not utilize the computation resources of the MEC server. On the other hand, it is found that, except for the TM curve, the other four W-shaped curves change relatively slowly and are close to the PMS, whereas the TM speed changes rapidly, and its average speed is obviously higher than others. This is expected due to different optimization objective function designs. At the same time, because of the higher average speed, which yields a higher data acquisition rate, the UAV of TM scheme needs to be closer to the BS to obtain a greater channel capacity, as shown in Fig. 4(a). It is also observed from Fig. 4(d) that, for large α , all the speed curves are one-peak shaped, and the average speeds are lower than those shown in Fig. 4(c). This is expected since with the large α , UAV has to slow down to obtain a lower data acquisition rate, especially when it is far away from BS. Only when closer to BS can UAV achieve a higher speed to decrease the MCT and propulsion energy consumption.

Fig. 5(a) depicts the UAV energy consumption of different schemes versus α . At first, it can be observed that for all schemes, the total energy consumption increases when α goes up. The EM and FP schemes achieve the lowest and highest consumption, respectively. It is shown that for small α , the performance of AO-energy scheme is close to that of the EM scheme. This is because that with sufficient channel capacity, the UAV prefers

to offload most of the data to obtain a lower energy consumption rather than compute them locally. However, as α goes up, the energy consumption of the AO-energy scheme drastically increases. The reason is that the UAV is unable to maintain the previous energy-efficient trajectory due to the relatively insufficient data processing capacity. Hence, the UAV has to slow down to decrease the data acquisition rate and be closer to the BS to obtain a better channel capacity, as mentioned before. It further causes longer flying distance and large energy consumption. In addition, it can be observed that for large α , the performance gap between EM and both PF and TM schemes is small. This is due to the fact when α is large, the resources allocation of $\{\mathbf{f}, \mathbf{p}\}$ tends to choose to their maximum value, which makes the performance of EM similar to PF and TM schemes, where $\{\mathbf{f}, \mathbf{p}\}$ is directly fixed as the maximum value. Furthermore, the PF and TM schemes are relatively close to the EM scheme within the entire range of α , which indicates that propulsion energy and MCT are the major components of the total UAV energy consumption. Fig. 5(b) compares the performance of different schemes versus B . We can observe that the impact of increasing B on the system energy performance is analogous to that of decreasing α . Hence, Fig. 5(b) shares similar characteristics with Fig. 5(a).

Figs. 6(a) and (b) illustrate the MCT consumption versus α and B , respectively. Note that there are no PF and FP schemes because they do not apply to the MCT optimization problem. It can be observed that TM scheme outperforms the other two schemes in these two figures, which demonstrates the effectiveness of Algorithm 3. Besides, one can observe that the performance gap between AO-time and TM schemes is remarkable when α is large or B is small, whereas the gap is tiny for the opposite cases.

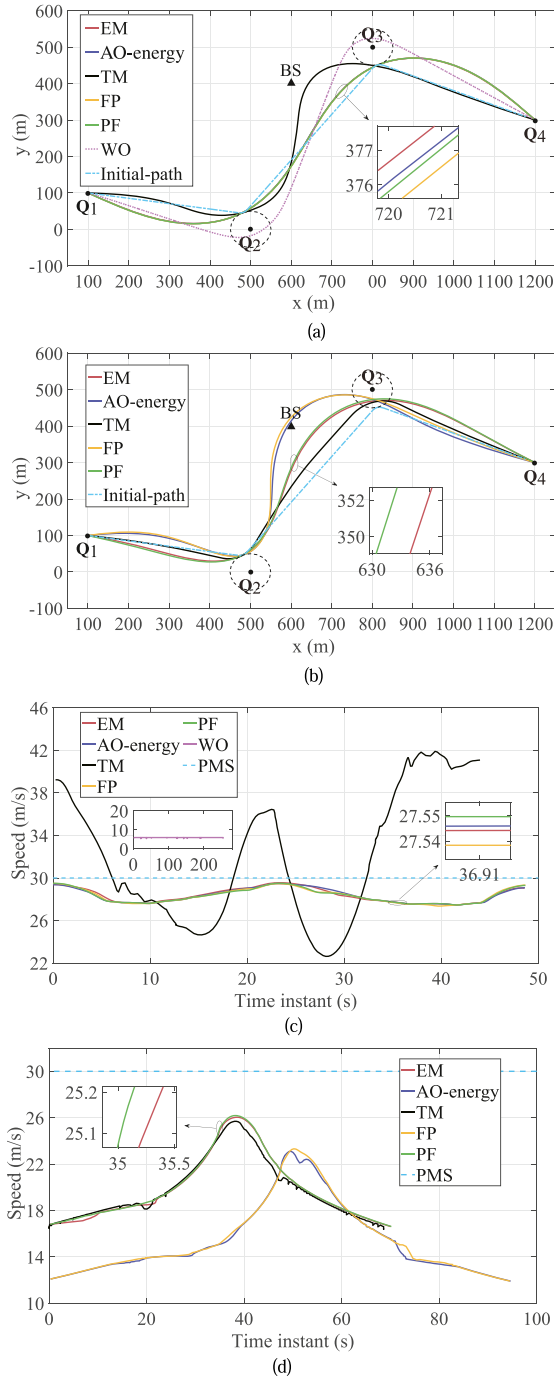


Fig. 4. UAV trajectories with different algorithms for different α . (a) Paths for $\alpha = 0.5 \times 10^6$ bit/m. (b) Paths for $\alpha = 1.7 \times 10^6$ bit/m. (c) Speeds versus time instant for Fig. 4(a). (d) Speeds versus time instant for Fig. 4(b).

This indicates that when the α is small or B is sufficiently large, offloading all data to the MEC server can achieve a small MCT consumption. At last, it is also observed that the performance gap between TM and EM schemes is becoming smaller as α increases or B decreases. This is because these two schemes tend to find similar solutions within diminishing feasible regions, as mentioned in the analysis of Fig. 5(a).

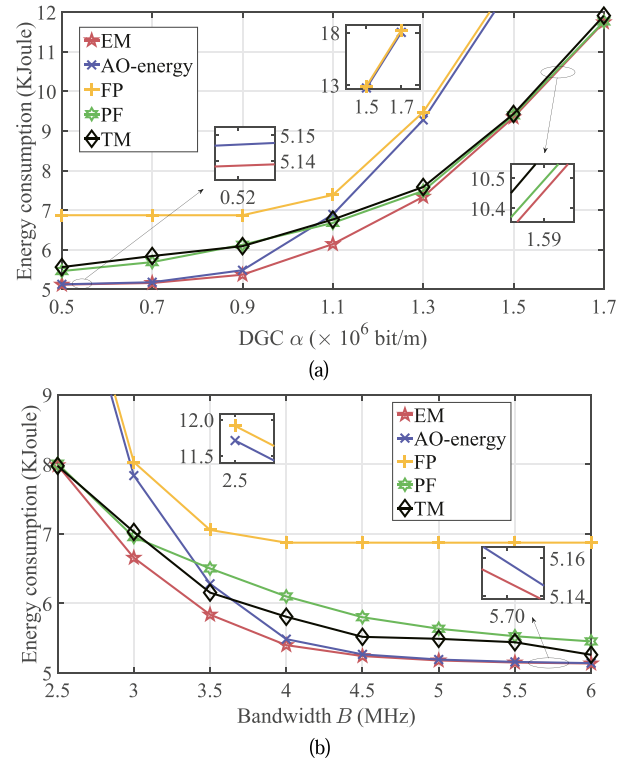


Fig. 5. UAV energy consumption with different algorithms versus different α and B . (a) Energy consumption versus different α . (b) Energy consumption versus different B .

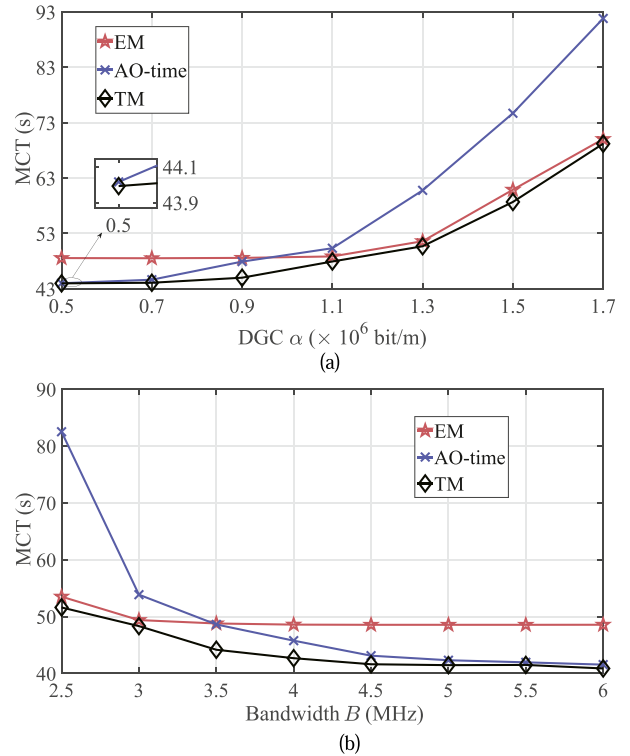


Fig. 6. MCT with different algorithms versus different α and B , where $\alpha = 1.2 \times 10^6$ bit/m. (a) MCT versus different α . (b) MCT versus different B .

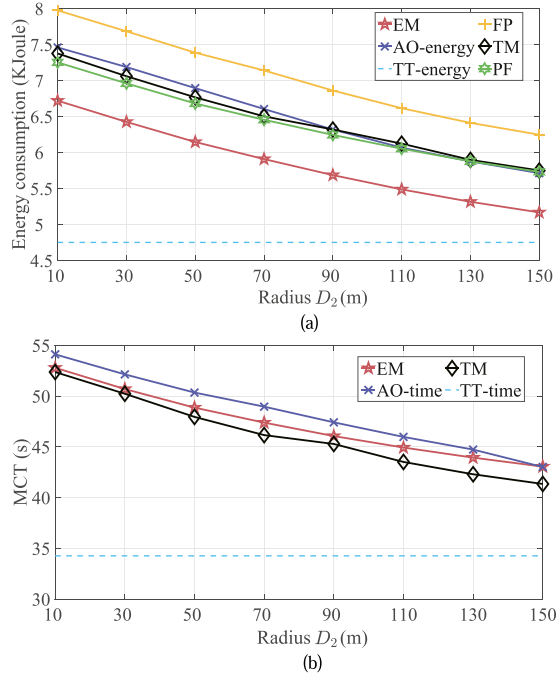


Fig. 7. Energy consumption and MCT versus different D_2 , where $D_3 = D_2$, $\alpha = 1.1 \times 10^9$ bit/m. (a) Energy consumption versus different D_2 . (b) MCT versus different D_2 .

In Fig. 7, we let $D_2 = D_3$,⁵ and compare the energy and MCT consumption of different schemes versus radius D_2 respectively. In the benchmarks *TT-energy* and *TT-time*, we omit the constraints $\|\mathbf{q}[N_k] - \mathbf{Q}_k\|_2 \leq D_k$, $\forall k = 2, 3$, in (25), i.e., there are only two target locations \mathbf{Q}_1 and \mathbf{Q}_4 . *TT-energy* and *TT-time* are then obtained by solving modified problems (P-2) and (P-7) with EM and TM algorithms, respectively. Firstly, it is shown that the EM and TM schemes outperform other schemes respectively in Fig. 7. It is found that the Y-axis values of all schemes in both Figs. 7(a) and (b) decrease as the radius increases. This is due to that, as the radius D_2 and D_3 increase, 1) the total flying distance can be shortened; 2) the UAV can move more freely to enjoy better communication channels (to the BS) and further reduce corresponding energy/time consumption. Last, it can be predicted that both the schemes EM and TM approach to the benchmarks *TT-energy* and *TT-time* as the radius D_2 and D_3 approach infinity, respectively.

VI. CONCLUSION

this article proposed a design that has the potential to help various applications utilizing UAV DA. We played emphasis on the real-time UAV data acquisition and processing with the assistance of MEC. To this design, we firstly constructed a novel UAV data acquisition rate model and then defined the real-time processing QoR. Next, the energy and MCT minimization problems were formulated, where the UAV trajectory, resources allocation, and time duration were jointly optimized with the constraints of real-time processing QoR, multiple locations,

⁵Actually, an end user can set different D_k based on the practical mission demands.

UAV mobility, and resources limitations. To conquer their high complexity, efficient iterative algorithms were proposed based on SCA and BCD techniques. For the resources allocation sub-problem, we rigorously derived a closed-form solution. Furthermore, so as to obtain a refined smooth trajectory initialization, we introduced a systematic and generic initialization method by utilizing Dubins curves. The numerical results showed that the MEC drastically enhanced the UAV real-time data acquisition and processing ability and our proposed algorithms significantly outperformed the benchmark schemes.

Considering the more practical channel models and investigating multi-UAV and multi-server scenarios are worthwhile future works.

APPENDIX A PROOF OF LEMMA 1

For the sake of conciseness, let $E(\mathbf{\Lambda})$ represent the objective function of problem (P-5.1). Firstly, note that $E(\mathbf{\Lambda})$ is differentiable strictly convex of $\mathbf{\Lambda}$ on \mathbb{R}_+^N , since it is a non-negative weighted sum of differentiable strictly convex functions of $\mathbf{\Lambda}$ on \mathbb{R}_+^N . The gradient of $E(\mathbf{\Lambda})$ can be obtained as

$$\nabla E(\mathbf{\Lambda}) = \left\{ \frac{\partial E}{\partial \lambda[n]} \right\} = \left\{ 3L\eta^3 \dot{\zeta}[n]^3 t[n] \lambda[n]^2 - \frac{t[n] \dot{\zeta}[n] \sigma^2}{Bh[n]} 2^{\frac{(1-\lambda[n])\dot{\zeta}[n]}{B}} \ln 2 \right\}. \quad (44)$$

It can be shown that

$$\begin{aligned} \nabla E(\mathbf{0}) &= \left\{ -\frac{t[n] \dot{\zeta}[n] \sigma^2}{Bh[n]} 2^{\frac{\dot{\zeta}[n]}{B}} \ln 2 \right\} \prec \mathbf{0}, \\ \nabla E(\mathbf{1}) &= \left\{ 3L\eta^3 \dot{\zeta}[n]^3 t[n] - \frac{t[n] \dot{\zeta}[n] \sigma^2}{Bh[n]} \ln 2 \right\} \succ \mathbf{0}, \end{aligned} \quad (45)$$

where (45) holds for general parameters settings. Since $E(\mathbf{\Lambda})$ is continuous and strictly convex on $\{\mathbf{0} \preceq \mathbf{\Lambda} \preceq \mathbf{1}\}$, there exists a unique root $\mathbf{\Lambda}_0$ of the equation $\nabla E(\mathbf{\Lambda}) = \mathbf{0}$ (as shown in (42)) in $\{\mathbf{0} \prec \mathbf{\Lambda} \prec \mathbf{1}\}$, based on the Intermediate Value Theorem and strict convexity. As a result, when restricted to any component $\lambda[n]$, $E(\mathbf{\Lambda})$ is monotonically decreasing in $[0, \lambda_0[n]]$ and monotonically increasing in $(\lambda_0[n], +\infty)$, we thus have

$$\lambda[n]^* = \begin{cases} \check{\lambda}[n], & \text{when } \lambda_0[n] \leq \check{\lambda}[n], \\ \hat{\lambda}[n], & \text{when } \hat{\lambda}[n] \leq \lambda_0[n], \\ \lambda_0[n], & \text{when } \check{\lambda}[n] < \lambda_0[n] < \hat{\lambda}[n], \end{cases}$$

which is equivalent to (39). By substituting $\mathbf{\Lambda}^*$ into (34) and (35), we can then obtain (40) and (41), respectively. This completes the proof.

REFERENCES

- [1] Y. Zeng and J. Tang, "Real-time data acquisition and processing under mobile edge computing-assisted UAV system," in *Proc. IEEE Glob. Commun. Conf.*, Rio de Janeiro, Brazil, 2022, pp. 1–6.
- [2] A. Fotouhi et al., "Survey on UAV cellular communications: Practical aspects, standardization advancements, regulation, and security challenges," *IEEE Commun. Surveys Tuts.*, vol. 21, no. 4, pp. 3417–3442, Fourthquarter 2019.

- [3] J. Wang, C. Jiang, Z. Han, Y. Ren, R. G. Maunder, and L. Hanzo, "Taking drones to the next level: Cooperative distributed unmanned-aerial-vehicular networks for small and mini drones," *IEEE Veh. Technol. Mag.*, vol. 12, no. 3, pp. 73–82, Sep. 2017.
- [4] J. Wang, C. Jiang, Z. Wei, C. Pan, H. Zhang, and Y. Ren, "Joint UAV hovering altitude and power control for space-air-ground IoT networks," *IEEE Internet Things J.*, vol. 6, no. 2, pp. 1741–1753, Apr. 2019.
- [5] Y. Zeng, Q. Wu, and R. Zhang, "Accessing from the sky: A tutorial on UAV communications for 5G and beyond," *Proc. IEEE*, vol. 107, no. 12, pp. 2327–2375, Dec. 2019.
- [6] A. Ollero, M. Tognon, A. Suarez, D. Lee, and A. Franchi, "Past, present, and future of aerial robotic manipulators," *IEEE Trans. Robot.*, vol. 38, no. 1, pp. 626–645, Feb. 2022.
- [7] K. Bodie et al., "Active interaction force control for contact-based inspection with a fully actuated aerial vehicle," *IEEE Trans. Robot.*, vol. 37, no. 3, pp. 709–722, Jun. 2021.
- [8] M. Tognon et al., "A truly-redundant aerial manipulator system with application to push-and-slide inspection in industrial plants," *IEEE Robot. Autom.*, vol. 4, no. 2, pp. 1846–1851, Apr. 2019.
- [9] J. Su et al., "Aerial visual perception in smart farming: Field study of wheat yellow rust monitoring," *IEEE Trans. Ind. Informat.*, vol. 17, no. 3, pp. 2242–2249, Mar. 2021.
- [10] R. Ke, Z. Li, J. Tang, Z. Pan, and Y. Wang, "Real-time traffic flow parameter estimation from UAV video based on ensemble classifier and optical flow," *IEEE Trans. Intell. Transp. Syst.*, vol. 20, no. 1, pp. 54–64, Jan. 2019.
- [11] L. Yang, J. Fan, Y. Liu, E. Li, J. Peng, and Z. Liang, "A review on state-of-the-art power line inspection techniques," *IEEE Trans. Instrum. Meas.*, vol. 69, no. 12, pp. 9350–9365, Dec. 2020.
- [12] J. Gong, T.-H. Chang, C. Shen, and X. Chen, "Flight time minimization of UAV for data collection over wireless sensor networks," *IEEE J. Sel. Areas Commun.*, vol. 36, no. 9, pp. 1942–1954, Sep. 2018.
- [13] J. Li et al., "Joint optimization on trajectory, altitude, velocity, and link scheduling for minimum mission time in UAV-aided data collection," *IEEE Internet Things J.*, vol. 7, no. 2, pp. 1464–1475, Feb. 2020.
- [14] C. Zhan and Y. Zeng, "Completion time minimization for multi-UAV-enabled data collection," *IEEE Trans. Wireless Commun.*, vol. 18, no. 10, pp. 4859–4872, Oct. 2019.
- [15] C. Zhan and Y. Zeng, "Aerial-ground cost tradeoff for multi-UAV-enabled data collection in wireless sensor networks," *IEEE Trans. Commun.*, vol. 68, no. 3, pp. 1937–1950, Mar. 2020.
- [16] B. Zhang, C. H. Liu, J. Tang, Z. Xu, J. Ma, and W. Wang, "Learning-based energy-efficient data collection by unmanned vehicles in smart cities," *IEEE Trans. Ind. Inform.*, vol. 14, no. 4, pp. 1666–1676, Dec. 2018.
- [17] C. Zhan, Y. Zeng, and R. Zhang, "Energy-efficient data collection in UAV enabled wireless sensor network," *IEEE Wireless Commun. Lett.*, vol. 7, no. 3, pp. 328–331, Jun. 2018.
- [18] J. Chen and J. Tang, "UAV-assisted data collection for dynamic and heterogeneous wireless sensor networks," *IEEE Wireless Commun. Lett.*, vol. 11, no. 6, pp. 1288–1292, Jun. 2022.
- [19] C. You and R. Zhang, "3D trajectory optimization in rician fading for UAV-enabled data harvesting," *IEEE Trans. Wireless Commun.*, vol. 18, no. 6, pp. 3192–3207, Jun. 2019.
- [20] M. Samir, S. Sharafeddine, C. M. Assi, T. M. Nguyen, and A. Ghrayeb, "UAV trajectory planning for data collection from time-constrained IoT devices," *IEEE Trans. Wireless Commun.*, vol. 19, no. 1, pp. 34–46, Jan. 2020.
- [21] H. Hu, K. Xiong, G. Qu, Q. Ni, P. Fan, and K. B. Letaief, "AoI-minimal trajectory planning and data collection in UAV-assisted wireless powered IoT networks," *IEEE Internet Things J.*, vol. 8, no. 2, pp. 1211–1223, Jan. 2021.
- [22] J. A. J. Berni, P. J. Zarco-Tejada, L. Suarez, and E. Fereres, "Thermal and narrowband multispectral remote sensing for vegetation monitoring from an unmanned aerial vehicle," *IEEE Trans. Geosci. Remote Sens.*, vol. 47, no. 3, pp. 722–738, Mar. 2009.
- [23] K. Uto, H. Seki, G. Saito, and Y. Kosugi, "Characterization of rice paddies by a UAV-mounted miniature hyperspectral sensor system," *IEEE J. Sel. Topics Appl. Earth Observ. Remote Sens.*, vol. 6, no. 2, pp. 851–860, Apr. 2013.
- [24] Z. Fan, J. Lu, M. Gong, H. Xie, and E. D. Goodman, "Automatic tobacco plant detection in UAV images via deep neural networks," *IEEE J. Sel. Topics Appl. Earth Observ. Remote Sens.*, vol. 11, no. 3, pp. 876–887, Mar. 2018.
- [25] E. Castelhão Tetila, B. Brandoli Machado, N. A. Belete, D. A. Guimarães, and H. Pistori, "Identification of soybean foliar diseases using unmanned aerial vehicle images," *IEEE Geosci. Remote Sens. Lett.*, vol. 14, no. 12, pp. 2190–2194, Dec. 2017.
- [26] G. J. Lim, S. Kim, J. Cho, Y. Gong, and A. Khodaei, "Multi-UAV pre-positioning and routing for power network damage assessment," *IEEE Trans. Smart Grid*, vol. 9, no. 4, pp. 3643–3651, Jul. 2018.
- [27] J. Zhu et al., "Urban traffic density estimation based on ultrahigh-resolution UAV video and deep neural network," *IEEE J. Sel. Topics Appl. Earth Observ. Remote Sens.*, vol. 11, no. 12, pp. 4968–4981, Dec. 2018.
- [28] Y. Pan, X. Zhang, G. Cervone, and L. Yang, "Detection of asphalt pavement potholes and cracks based on the unmanned aerial vehicle multispectral imagery," *IEEE J. Sel. Topics Appl. Earth Observ. Remote Sens.*, vol. 11, no. 10, pp. 3701–3712, Oct. 2018.
- [29] Y. Geng et al., "UAV-LiDAR-based measuring framework for height and stagger of high-speed railway contact wire," *IEEE Trans. Intell. Transp. Syst.*, vol. 23, no. 7, pp. 7587–7600, Jul. 2022.
- [30] Z. Zhou et al., "When mobile crowd sensing meets UAV: Energy-efficient task assignment and route planning," *IEEE Trans. Commun.*, vol. 66, no. 11, pp. 5526–5538, Nov. 2018.
- [31] J. Yao and N. Ansari, "QoS-aware rechargeable UAV trajectory optimization for sensing service," in *Proc. IEEE Int. Conf. Commun.*, Shanghai, China, 2019, pp. 1–6.
- [32] S. Zhang, H. Zhang, Z. Han, H. V. Poor, and L. Song, "Age of information in a cellular internet of UAVs: Sensing and communication trade-off design," *IEEE Trans. Wireless Commun.*, vol. 19, no. 10, pp. 6578–6592, Oct. 2020.
- [33] N. Zhao et al., "UAV-assisted emergency networks in disasters," *IEEE Wireless Commun.*, vol. 26, no. 1, pp. 45–51, Feb. 2019.
- [34] M. Hua, Y. Huang, Y. Wang, Q. Wu, H. Dai, and L. Yang, "Energy optimization for cellular-connected multi-UAV mobile edge computing systems with multi-access schemes," *J. Commun. Inf. Netw.*, vol. 3, no. 4, pp. 33–44, Dec. 2018.
- [35] J. Zhou, D. Tian, Z. Sheng, X. Duan, and X. Shen, "Joint mobility, communication and computation optimization for UAVs in air-ground cooperative networks," *IEEE Trans. Veh. Technol.*, vol. 70, no. 3, pp. 2493–2507, Mar. 2021.
- [36] X. Cao, J. Xu, and R. Zhang, "Mobile edge computing for cellular-connected UAV: Computation offloading and trajectory optimization," in *Proc. IEEE Int. Workshop Signal Process. Adv. Wireless Commun.*, Kalamata, Greece, 2018, pp. 1–5.
- [37] S. Huang, L. Li, Q. Pan, W. Zheng, and Z. Lu, "Fine-grained task offloading for UAV via MEC-enabled networks," in *Proc. IEEE Int. Symp. Pers., Indoor Mobile Radio Commun.*, Istanbul, Turkey, 2019, pp. 1–6.
- [38] D. Callegaro and M. Levorato, "Optimal edge computing for infrastructure-assisted UAV systems," *IEEE Trans. Veh. Technol.*, vol. 70, no. 2, pp. 1782–1792, Feb. 2021.
- [39] T. Bai, J. Wang, Y. Ren, and L. Hanzo, "Energy-efficient computation offloading for secure UAV-edge-computing systems," *IEEE Trans. Veh. Technol.*, vol. 68, no. 6, pp. 6074–6087, Jun. 2019.
- [40] X. Gu, G. Zhang, and J. Gu, "Offloading optimization for energy-minimization secure UAV-edge-computing systems," in *Proc. IEEE Wirel. Commun. Netw. Conf.*, Nanjing, China, 2021, pp. 1–6.
- [41] F. Luo, C. Jiang, S. Yu, J. Wang, Y. Li, and Y. Ren, "Stability of cloud-based UAV systems supporting Big Data acquisition and processing," *IEEE Trans. Cloud Comput.*, vol. 7, no. 3, pp. 866–877, Jul.–Sep. 2019.
- [42] H. Huang and A. V. Savkin, "An algorithm of reactive collision free 3-D deployment of networked unmanned aerial vehicles for surveillance and monitoring," *IEEE Trans. Ind. Inform.*, vol. 16, no. 1, pp. 132–140, Jan. 2020.
- [43] Y. Zeng, X. Xu, and R. Zhang, "Trajectory design for completion time minimization in UAV-enabled multicasting," *IEEE Trans. Wireless Commun.*, vol. 17, no. 4, pp. 2233–2246, Apr. 2018.
- [44] J. Zhang, Y. Zeng, and R. Zhang, "UAV-enabled radio access network: Multi-mode communication and trajectory design," *IEEE Trans. Signal Process.*, vol. 66, no. 20, pp. 5269–5284, Oct. 2018.
- [45] Y. Zeng and R. Zhang, "Energy-efficient UAV communication with trajectory optimization," *IEEE Trans. Wireless Commun.*, vol. 16, no. 6, pp. 3747–3760, Jun. 2017.
- [46] W. Yuan and K. Nahrstedt, "Energy-efficient CPU scheduling for multimedia applications," *ACM Trans. Comput. Syst.*, vol. 24, no. 3, pp. 292–331, Aug. 2006.
- [47] A. R. Jensen, M. Lauridsen, P. Mogensen, T. B. Sørensen, and P. Jensen, "LTE UE power consumption model: For system level energy and performance optimization," in *Proc. IEEE Veh. Technol. Conf.*, Quebec City, QC, Canada, 2012, pp. 1–5.
- [48] Y. Zeng, J. Xu, and R. Zhang, "Energy minimization for wireless communication with rotary-wing UAV," *IEEE Trans. Wireless Commun.*, vol. 18, no. 4, pp. 2329–2345, Apr. 2019.

- [49] S. Boyd and L. Vandenberghe, *Convex Optimization*. Cambridge, U.K.: Cambridge Univ. Press, 2004.
- [50] B. R. Marks and G. P. Wright, "A general inner approximation algorithm for non-convex mathematical programs," *Oper. Res.*, vol. 26, no. 4, pp. 681–683, Jul. 1978.
- [51] C. Chen, Y. He, C. Bu, J. Han, and X. Zhang, "Quartic bézier curve based trajectory generation for autonomous vehicles with curvature and velocity constraints," in *Proc. IEEE Int. Conf. Robot. Autom.*, Hong Kong, China, 2014, pp. 6108–6113.
- [52] L. E. Dubins, "On curves of minimal length with a constraint on average curvature, and with prescribed initial and terminal positions and tangents," *Amer. J. Math.*, vol. 79, no. 3, pp. 497–516, Jul. 1957.



Yao Zeng (Student Member, IEEE) received the B.E. degree in process equipment and control engineering in 2020, from the School of Mechanical and Automotive Engineering, South China University of Technology, Guangzhou, China, where he is currently working towards the M.E. degree with the Shien-Ming Wu School of Intelligent Engineering. His research interests include edge computing, motion planning, and UAV communication.



Jianhua Tang (Member, IEEE) received the B.E. degree in communications engineering from Northeastern University, Shenyang, China, in 2010, and the Ph.D. degree in electrical and electronic engineering from Nanyang Technological University, Singapore, in 2015. He was a Postdoctoral Research Fellow with the Singapore University of Technology and Design, Singapore, from 2015 to 2016, and Research Assistant Professor with the Department of Electrical and Computer Engineering, Seoul National University, Seoul, South Korea, from 2016 to 2018. He is currently an Associate Professor with the Shien-Ming Wu School of Intelligent Engineering, South China University of Technology, Guangzhou, China. His research interests include edge computing, network slicing, and industrial Internet of Things. He was the recipient of the 2020 IEEE Communications Society Stephen O. Rice Prize. He is also the Editor of the IEEE WIRELESS COMMUNICATIONS LETTERS.